

# Collective chemotactic search strategies

Hugues Meyer,<sup>1,\*</sup> Adam Wysocki,<sup>1,†</sup> and Heiko Rieger<sup>1,‡</sup>

<sup>1</sup>*Department of Theoretical Physics & Center for Biophysics,  
Saarland University, 66123 Saarbrücken, Germany*

(Dated: September 27, 2024)

Chemotactic biological or synthetic active matter shapes its environment by secretions of chemical signals from its self-propelled constituents, like cells, organisms or active colloids. From this indirect interaction collective effects emerge that can be used by the agents to migrate collectively, to form patterns or to search for targets more efficiently. Here, we use paradigmatic models to study the efficiency of collective search strategies of a large group of motile agents that release during their movement repulsive auto-chemotactic signals forcing them to move away from high concentrations of the chemical clue. We show that the repulsive chemotactic interactions improve the search efficiency, measured by the mean first passage time to find a randomly located target, by orders of magnitude depending on the strength of the chemotactic coupling. The mechanism for this improvement relies on two factors: the increase of the persistence length due to the agent's self-interaction with its own chemotactic field *and* by a more homogeneous distribution of the agents due to their mutual indirect repulsion mediated by the chemotactic field. At stronger particle-field coupling the chemotactic searchers self-organize into ballistically moving bands reminiscent of search-chains formed in search and rescue operations, whose efficiency depends on the number of searchers involved. Our comprehensive study of collective search strategies of large groups of interacting agents is not only relevant for chemotactic active matter but also for a wide range of fields like ethology, information engineering, robotics, and social engineering.

## I. INTRODUCTION

Chemotaxis is the ubiquitous mechanism by which organisms, cells or bacteria direct their movements according to certain chemicals in their environment by responding to a gradient in the concentration field of a chemical species. When this gradient is generated by the organisms themselves, this response is denoted as autochemotaxis and is one way in which organisms exchange information by leaving chemical cues along their paths as they search, which can be later sensed by fellow searchers and used to influence their motion, in analogy to what ants do to organize their traffic [1]. Prominent examples in cell biology are migrating cells during embryogenesis [2], immune responses [3], and neural pathfinding [4].

Self-generated gradients by attractant breakdown even allow cells to make long-range route decisions and navigate through complex environments [5, 6] and cells can leave long-lived physicochemical footprints along their way, which determine their future path [7]. Recently, chemotactic interactions have also been realized in synthetic matter, like self-propelled microdroplets that communicate via chemorepulsive trails [8], showing self-caging, or colloidal particles that leave phase-change trails [9], mimicking tunable pheromone interactions as among ants. Synthetic chemotaxis in active matter systems generically lead to pattern formation like dynamic

clusters and waves [10–12] and has recently been studied intensively [13–18]. Moreover, it is a natural example of non-reciprocal interactions, i.e. interactions that violate the *actio=reactio* principle and that became recently a major research focus [19–23].

Positive autochemotaxis is frequently connected with cell aggregation [24], whereas repulsive signaling in negative autochemotaxis can be connected to efficient space exploration, for instance for mutual avoidance during efficient foraging of ants [25]. How efficient chemotactic repulsion actually performs in the search for randomly located targets remains elusive - which is what we intend to address in this paper: a quantitative analysis of the efficiency of stochastic search processes with autochemotactic repulsion. Search processes are ubiquitous in nature, society and daily life, a comprehensive classification from a game theoretic and robotic perspective can be found in [26]. Physically relevant search processes are often stochastic in nature [27–29] and include chemical reaction kinetics [30–32], genetic transcription [33, 34], bacteria searching for nutrients [35] or immune cells searching for pathogenic cells [36], foraging animals [37–40] or swarming robots [41, 42], to name but a few. The efficiency of a specific search process is usually measured in the mean first passage time (MFPT) [28], the average time needed to reach the target for the first time, but also other cost factors may contribute [43], in particular when multiple searchers are involved.

Most search processes share the need to be optimized in a way such that searchers reach the target as fast as possible or with the least amount of resources, which then defines an optimal search strategy. Over the past two decades, the analysis of such optimal search strategies has attracted a lot of interest and were studied for var-

---

\* hugues.meyer@uni-saarland.de; These authors contributed equally to this work.

† a.wysocki@lusi.uni-sb.de; These authors contributed equally to this work.

‡ heiko.rieger@uni-saarland.de

ious search processes like for instance Lévy flights [44] and intermittent walks [45], persistent random walks [46] and random walks with  $n$ -step memory [47, 48], random walks with resetting [49–53], and random walks interacting with the environment [54].

These search strategies were up to now limited to a single searcher. The MFPT for an  $N$ -agent search has frequently been studied for *independent*, i.e. non-interacting searchers, sometimes also denoted as the lion-and-the-lamb problem [55–60], with the general and plausible result that  $N$  searcher find the target faster and that their optimal search strategy is generally identical to the optimal single-searcher strategy. Very few works have investigated the search performances of interacting agents in specific simple systems, e.g. via an instantaneous 2-body potential in an one dimensional [61] or dilute system [62], or in the context of acoustic communication [63], all of them predicting an optimal repulsive interaction range. However, in how far interactions or communication between random searchers and their resulting collective behaviours can lead to improved *collective* search strategies has not been systematically studied so far and general principles remains elusive.

In this work we will study to which extent auto-chemotactically interacting, but otherwise stochastically moving, searchers are efficient to find a randomly located target. Our theoretical framework comprises paradigmatic models for a large number,  $N$ , of randomly moving particles producing a diffusive, chemotactically repulsive trail. The emerging stochastic process is non-Markovian [47] and constitutes effectively an interacting many-body problem, which is impossible to study analytically without serious approximations, for which reason we predominantly use computer simulations. The main quantity characterising the search efficiency of these interacting  $N$ -particle search processes will be the MFPT. We will show that optimal search strategies exist, i.e. optimal choices for the specific parameters defining the stochastic processes, which minimize the MFPT for a fixed number,  $N$ , of searchers, and that are substantially better than that of independent searchers due to collective effects.

The paper is organized as follows: in section II the models are introduced, in section III the search process for single searchers are recapitulated, section IV and V contain the analysis of the  $N$ -agent search with and without self-interaction, respectively. Section VI concludes with a discussion and an outlook.

## II. MODELS

We consider chemotactically interacting, self-propelled particles, like migrating cells or foraging ants, and describe them by a stochastic processes for the position of the particles and a deterministic diffusion equation with moving sources for the chemotactic field. Negative autochemotaxis means that particles tend to move away from areas with high concentrations of the chemo-

tactic field, which we model in two ways to identify the universal aspects of collective effects induced by chemo-repulsive interactions: first with an active Brownian particle model (ABP) [64, 65] with repulsive auto-chemotaxis, which has been introduced and studied for attractive auto-chemotaxis in [66], and second with a lattice model that is inspired by the true self-avoiding random walk [67] to which the chemical diffusion of the trail is added [47]. The difference between the two models is that the ABP model allows for a continuous change of the particle direction away from a concentration gradient of the chemotactic field, whereas the random walk model allows for instantaneous directional changes towards the smallest concentration of the chemotactic field.

### A. Auto-chemotactic Active Brownian particles (ACP)

The auto-chemotactic active Brownian particle (ACP) model consists of active Brownian particles emitting a diffusive chemical cue that serves as a chemotactic signal for all particles. We adapt the model introduced in [66, 68] for autochemotaxis:  $N$  self-propelled, disk-like (radius  $a$ ) particles move in two space dimensions according to

$$\dot{\mathbf{r}}_i(t) = v_0 \mathbf{e}_i(t) + \sum_{j=1}^N \frac{\mathbf{f}(r_{ij})}{\gamma_t}, \quad (1)$$

where  $\mathbf{r}_i(t)$  is the position of particle  $i$  at time  $t$ ,  $v_0$  is the self-propulsion velocity,

$$\mathbf{e}_i(t) = \begin{pmatrix} \cos \varphi_i(t) \\ \sin \varphi_i(t) \end{pmatrix} \quad (2)$$

the propulsion direction with polar angle  $\varphi_i(t)$ ,  $\gamma_t$  the translational friction constant,  $r_{ij} = |\mathbf{r}_i(t) - \mathbf{r}_j(t)|$  the distance between particle  $i$  and  $j$ , and  $\mathbf{f}(r_{ij})$  a harmonic repulsive force of the form:  $f(r) = f_0(2 - r/a)$  for  $r \leq 2a$  and zero otherwise, where  $f_0$  measures the particle stiffness.

Each particle produces a chemical cue with a rate  $h_c$ , which diffuses into the environment with diffusion constant  $D_c$ , and decays with a rate  $k_c$ , so that its concentration  $c(\mathbf{r}, t)$  obeys the inhomogeneous diffusion equation

$$\dot{c}(\mathbf{r}, t) = D_c \Delta c(\mathbf{r}, t) - k_c c(\mathbf{r}, t) + h_c \sum_{i=1}^N \delta(\mathbf{r} - \mathbf{r}_i(t)). \quad (3)$$

Chemotaxis is the ability of active agents to control their direction of motion, in the ACP model defined by the angles  $\varphi_i(t)$ , in response to a chemical stimulus. We model such a response by a torque that tries to align or *anti*-align their direction of motion with the gradient of the concentration field:

$$\dot{\varphi}_i(t) = \frac{\kappa}{\gamma_r} [\nabla c(\mathbf{r}_i(t), t) \times \mathbf{e}_i(t)]_z + \sqrt{2D_r} \eta_i(t), \quad (4)$$

where the cross product of  $\nabla c$  with  $\mathbf{e}_i$  points perpendicular to the 2d plane along the  $z$ -axis,  $\gamma_r$  is a rotational friction constant and  $\kappa$  a chemotactic sensitivity.

For  $\kappa > 0$  the particle *anti-align* with  $\nabla c$  and the model describes chemo-repulsion, which we consider here. On the other hand, for  $\kappa < 0$  the particle aligns with  $\nabla c$  and the model describes chemo-attraction, which was considered in [68]. The second term on the r.h.s. is the usual rotational noise for ABPs with  $D_r$  the rotational diffusion constant and  $\eta_i(t)$  Gaussian white noise with  $\langle \eta_i(t) \rangle = 0$  and  $\langle \eta_i(t) \eta_j(t') \rangle = \delta_{ij} \delta(t - t')$ .

To avoid strong self-interaction, we locate the sensor measuring the gradient in the front of the particle at  $\mathbf{r}_i + a\mathbf{e}_i$  and the source, which is approximated by a Gaussian function [69], in the back at  $\mathbf{r}_i - a\mathbf{e}_i$ . We scale lengths by the radius  $a$  and time by the propulsion time  $v_0/a$ . For convenience we define a new chemotactic sensitivity  $\beta = \kappa/\gamma_r$ . Important dimensionless numbers are the packing fraction  $\phi = \pi a^2 N/L^2$ , persistence length of motion  $l_p = v_0/(aD_r)$  and chemotactic coupling  $\Lambda = \beta h_c a/D_c^2$ .

We use a simulation box of size  $L/a = 100$  with periodic boundary conditions in all directions. We vary the decay rate from  $k_c a/v_0 = 0$  to 0.2, the apersistence length from  $l_p = 0.5$  to 5, the chemotactic sensitivity from  $\beta/(v_0 a^2) = 0.0125$  to 2.5, the diffusion constant from  $D_c/(v_0 a) = 0.005$  to 100 and the source strength from  $h_c a/v_0 = 50$  to 4000. We integrate the equations of motion (1, 2, 4) numerically using Brownian dynamics simulation and the diffusion equation (3) with an alternating-direction implicit method [70].

## B. Auto-chemotactic walker (ACW)

The auto-chemotactic random walk (ACW) model is defined on a lattice and contains the main ingredients of auto-chemotaxis [18].  $N$  walkers are placed on sites of a 2-dimensional lattice and a concentration field  $c^{(l)}$  is defined for each walker  $l$ , its value on a site  $i$  at time  $t$  being denoted  $c_i^{(l)}(t)$ . The total concentration field  $c$  is defined as the sum of all fields, i.e.,  $c_i(t) = \sum_{l=1}^N c_i^{(l)}(t)$ .

The time evolution of the system is governed by a master equation for the probability  $\rho_i(t)$  of a walker to be found on site  $i$  at time  $t$ ,

$$\rho_i(t+1) = \sum_{j \in \mathcal{N}_i} p_{j \rightarrow i}(t) \rho_j(t), \quad (5)$$

as the walkers jump at constant time intervals  $\Delta t = 1$ , where the probability  $p_{j \rightarrow i}$  to jump from site  $j$  to site  $i$  is given by

$$p_{j \rightarrow i}(t) = \frac{e^{-\beta c_i(t)}}{\sum_{k \in \mathcal{N}_j} e^{-\beta c_k(t)}} \quad (6)$$

and  $\mathcal{N}_i$  is the set of neighboring sites of  $i$ .

Simultaneously, the concentration field evolves according to a standard diffusion equation, i.e.,

$$\dot{c}_i^{(l)}(t) = D_c \sum_{j \in \mathcal{N}_i} [c_j^{(l)}(t) - c_i^{(l)}(t)] + h_c \sum_{\tau=0}^{\infty} \sum_{n=1}^N \delta_{in} \delta(t-\tau), \quad (7)$$

where the sum of the source terms runs over all particles and  $\delta_{in} = 1$  if the particle is located on the site  $i$  and 0 otherwise. The term  $\delta(t-\tau)$  indicates that the deposition of the cue occurs at constant intervals  $\Delta t = 1$ .

The model contains three main parameters. First, the deposition rate  $h_c$ . We define it as a unit of concentration per unit time and therefore use  $h_c = 1$  throughout this study. Then, the diffusion constant  $D_c$ . For  $D_c = 0$ , any amount of chemical deposited on a site remains there forever, and the model becomes the well-known true self-avoiding walk [67]. Finally, the chemotactic coupling strength  $\beta$ . For  $\beta = 0$ , the walkers are insensitive to the concentration field and jump to any neighboring site with the same probability. On the other hand, for  $\beta \rightarrow \infty$  the walkers always jump to the neighboring site with the lowest concentration.

We simulate this model by means of Monte-Carlo simulations on a 2-dimensional square lattice of size  $L \times L = 100 \times 100$ . The diffusion equation for the concentration field is integrated using the Crank-Nicolson method [70] and the diffusion coefficient is chosen as  $D_c = 0.5$  in most simulations.

## C. Mean first-passage time (MFPT) computation

The event for which the MFPT is computed is defined to be the first encounter of one of the  $N$  particles with a randomly located target, where encounter means overlap of the particle disk with the target position in the continuum and jump to the target site on the lattice. Initially, all searchers are placed randomly in the simulation box and the concentration field is set to zero everywhere. The simulations are then run until the system reaches its steady-state. Then, targets are introduced in the system.

In the ACP model, we randomly distribute immobile targets (disks with radius  $a$ ) in the simulation box and measure for each target the time it takes to be touched by a searcher for the first time. After the target is found, it is moved to a new random location and its clock is reset to zero. This gives us an estimator of the survival function  $S_N(t)$ , i.e., the probability that the lifetime  $T$  of a target in the presence of  $N$  searchers is greater than  $t$ , from which we compute the MFPT as

$$\bar{T}_N = \int_0^{\infty} S_N(t) dt. \quad (8)$$

In the ACW model, we record for each site  $i$  of a set of  $N_s$  randomly selected sites the time  $\tau_i$  at which a first walker reaches it. Because all sites are equivalent, all  $N_s \times N_t$  times  $\tau_i$  are used to evaluate the first-passage

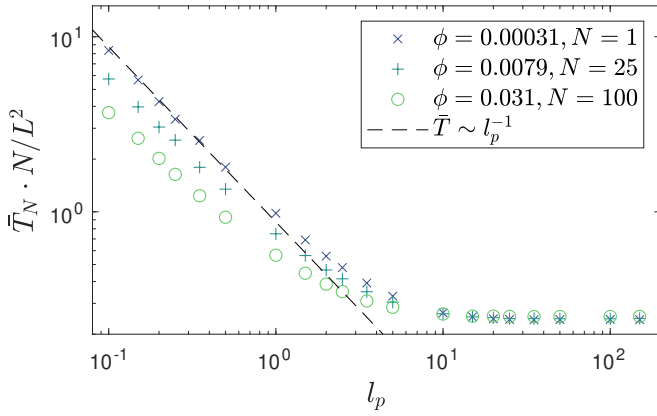


FIG. 1. Mean first-passage time (MFPT)  $\bar{T}_N$  of active Brownian particles without coupling to the chemotactic field ( $\beta = 0$ ) as a function of the persistence length  $l_p = v_0/(aD_r)$  for different packing densities  $\phi$ . Time is defined in units of the propulsion time  $a/v_0$  and lengths in units of the particle radius  $a$ .

distribution and its mean, where  $N_t$  is the number of trajectories run.

### III. THE SINGLE-AGENT SEARCH

To identify collective effects in the search efficiency of an  $N$ -particle system one needs to compare it with the search efficiency of  $N$  independent (non-interacting) particles, which derives from the single-agent search MFPT, which is calculated in this section.

#### A. Single ACP

Already the movement of a single autochemotactic particle is influenced its own chemotactic field, for which reason we need to compare its MFPT with the one of the process without chemotaxis ( $\beta = 0$ ). By varying the persistence length  $l_p$ , we find that MFPT (in units of propulsion time  $a/v_0$ ) scales as  $\bar{T} \sim l_p^{-1}$  in the Brownian regime ( $l_p < 1$ ) and is constant for persistent particles ( $l_p \gg 1$ ), c.f. Fig. 1.

Next the chemotactic coupling is switched on ( $\beta > 0$ ) and for all parameter combinations ( $l_p, \beta, D_c, k_c, h_c$ ) the effective rotational diffusion constant  $D_r^{\text{eff}}$  is extracted from the decay of the orientation auto-correlation function  $\langle \mathbf{e}(0) \cdot \mathbf{e}(t) \rangle = \exp(-D_r^{\text{eff}} t)$ . There is not a simple dependence of  $D_r^{\text{eff}}$  on the model parameters, but Fig. 2(a) shows that the scaling variables  $(\sqrt{D_r^{\text{eff}}/D_r} - 1)/\Lambda$  form a master curve when plotted against  $\zeta = (4D_c)^{-1} + k_c$  as predicted in the weak chemotactic coupling limit in [68].

If only the diffusion constant of the chemotactic field,  $D_c$ , is varied, and all other parameters held fixed, the effective rotational diffusion constant of the particle is  $D_r^{\text{eff}} = D_r$  for very large and very small  $D_c$  with a mini-

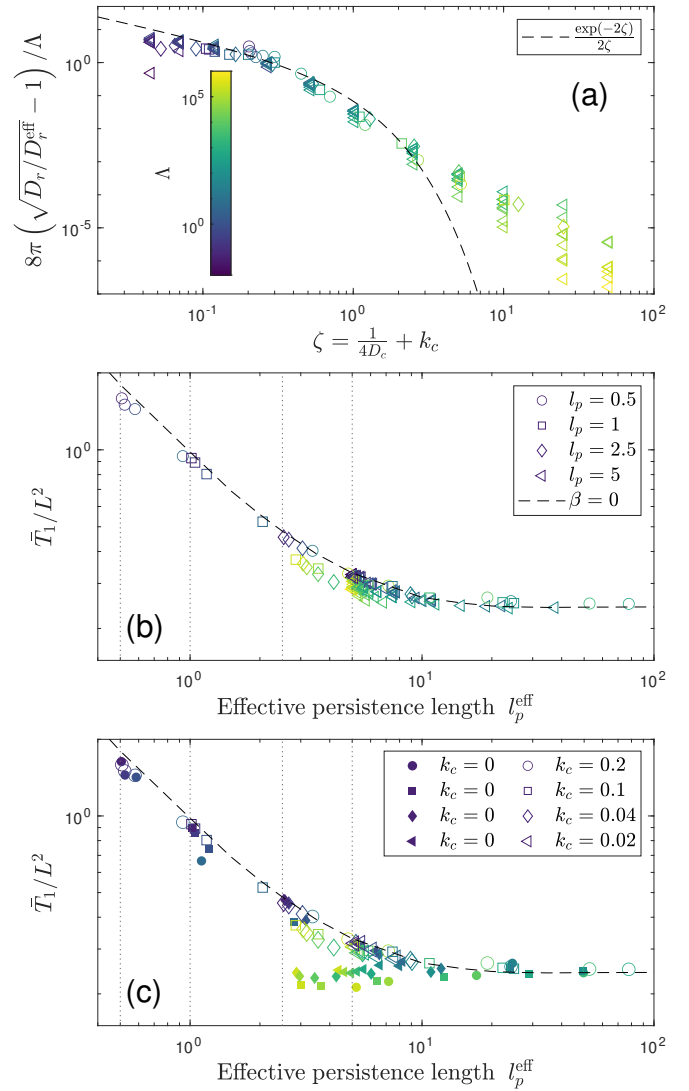


FIG. 2. Single ACP: (a) Scaling plot of the effective rotational diffusion constant  $D_r^{\text{eff}}$  for different bare persistence lengths  $l_p$  (different symbols) and varying dimensionless coupling constants  $\Lambda = \beta h_c a / D_c^2$  (color code). The dashed line is the analytical expression for the weak chemotactic coupling [68]. (b) MFPT  $\bar{T}_1$  as function of the effective persistence length  $l_p^{\text{eff}} = l_p D_r / D_r^{\text{eff}}$  for different bare persistence lengths  $l_p = v_0/(aD_r)$ . The vertical dotted lines indicate the bare persistence lengths  $l_p$ . (c) MFPT  $\bar{T}_1$  as function of the effective persistence length  $l_p^{\text{eff}}$  for different decay rates  $k_c > 0$  (open symbols) of the chemotactic field  $c$  with the MFPT for vanishing decay rate  $k_c = 0$  (full symbols). Parameters are as in (b). Note the significant improvement of the MFPT for  $k_c = 0$  for high chemotactic coupling  $\Lambda$  (large  $l_p^{\text{eff}}$ ) due to long-term memory of the chemical field.

mum in between. This is because at large  $D_c$  gradients in the concentration  $c$  disappear fast and thus the chemotactic response is low. On the other hand, for very small  $D_c$ , the particle has to circle around to cross its own trail, which usually takes longer than  $1/D_r$  and thus has no influence on the rotational dynamics.

Using the effective rotational diffusion constant one can define an effective persistence length  $l_p^{\text{eff}} = l_p D_r / D_r^{\text{eff}}$  and Fig. 2(b) shows the MFPT  $\bar{T}_1$  as a function of  $l_p^{\text{eff}}$  for different bare persistent lengths  $l_p = v_0 / (a D_r)$  in comparison with the result of a simple active Brownian particle ( $\beta = 0$ ). Fig. 2(c) shows that for non-vanishing decay constant  $k_c \neq 0$ , the dependence of the MFPT on the effective persistence length  $l_p^{\text{eff}}$  is nearly identical to the one of a simple active Brownian particle on the bare persistence length  $l_p$  and decays as  $\bar{T} \sim (l_p^{\text{eff}})^{-1}$  in the Brownian regime and is constant for persistent particles. This implies that for the parameter considered here the self-generated chemical signal only modifies the persistence of the motion and has no other effect on the search efficiency.

Fig. 2(c) also shows that the situation is different for  $k_c = 0$ , i.e. a chemical trail is not destroyed by a decay process: long-time memory emerges leading to a significant improvement in search efficiency for large chemotactic coupling  $\Lambda = \beta h_c a / D_c^2$ , c.f. the solid and open symbols for  $k_0 = 0$  and  $k_c \neq 0$ , respectively, for in the regime of intermediate effective persistence length  $2 < l_p^{\text{eff}} < 10$ .

### B. Single ACW

The single ACW has been analyzed in [47] where it was shown that the MFPT  $\bar{T}_1$  decreases with the chemotactic coupling  $\beta$  for small  $\beta$  and increases sharply for large  $\beta$ , such that it displays a minimum at some value  $\beta^*$ , which is the optimal search strategy for the single ACW, c.f. Fig. 3(a). For large values of  $\beta$  the particle trajectories are straight lines, which on a square have only two directions and therefore miss the target with high probability leading to a diverging MFPT. This is different in the ACP model, where ballistically moving particles can go in any direction in two-dimensional space leading to a constant but finite MFPT for periodic boundary conditions.

Here we demonstrate that the MFPT  $\bar{T}$  is a function of the (numerically computed) persistence length  $l_p$  (average number of consecutive steps taken in the same direction) alone, as shown in Fig. 3(b). The persistence length defines a persistent random walk, for which it can be adjusted to minimize the MFPT [46]. For the ACW considered here the persistence length  $l_p$  increases monotonically with the chemotactic coupling since as  $\beta$  increases, the walker tends to jump to the neighbouring site with the lowest concentration with less and less fluctuations, which eventually results in a purely ballistic motion [18]. There exists hence a value of  $\beta$  for which the resulting persistence length  $l_p$  is optimal for the search. We note that this optimal value  $\beta^*$  depends non-trivially on the diffusion constant  $D_c$  as  $l_p$  also depends on  $D_c$  in a non-monotonous way, see [18] for details. We therefore observe that  $\beta^*$  first decreases with  $D_c$  for low values of  $D_c$ , then reaches a minimum and eventually increase again for large values of  $D_c$ , see Fig. 3(c).

To check whether there are other effects besides a

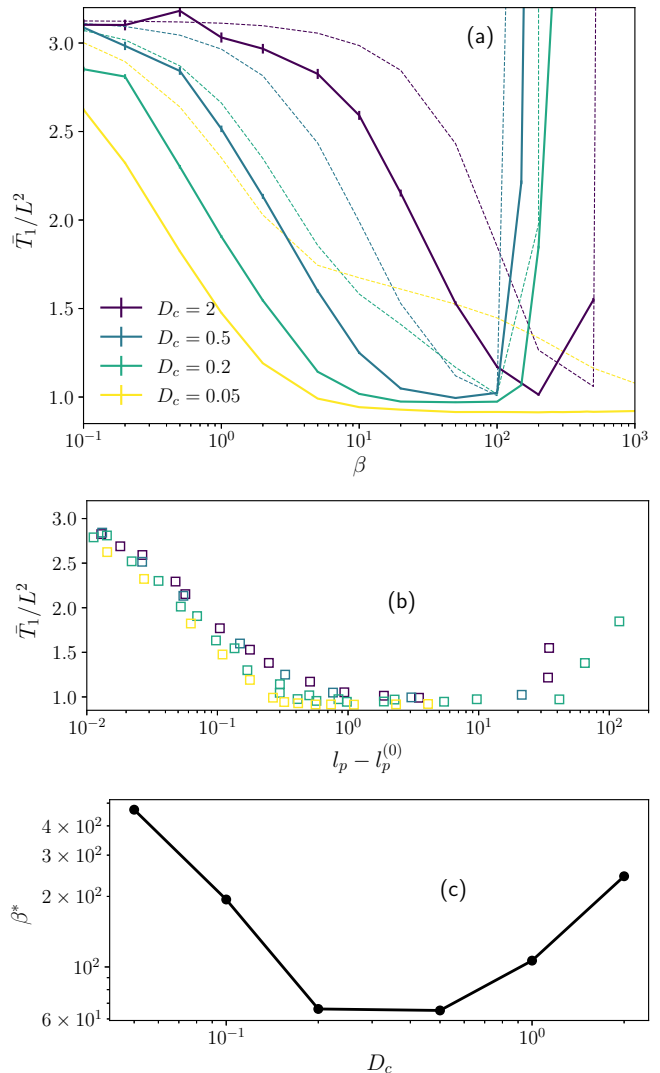


FIG. 3. Single ACW: (a) MFPT  $\bar{T}$  of a single chemotactic random walker as a function of the coupling constant  $\beta$ . Solid line are the results of the full model for various values of  $D_c$ . The dashed lines are the results of the effective model, where the transition probabilities  $p_{\rightarrow, \uparrow, \leftarrow, \downarrow}$  are measured in the simulations. (b) MFPT  $\bar{T}$  as a function of the measured persistence length  $l_p$  from which we have subtracted its value for a blind random walk  $l_p^{(0)} = 4/3$ . (c) Optimal values of the chemotactic coupling  $\beta$  as a function of  $D_c$ .

change in the persistence length that govern the search in our model, we extract the relative frequencies of forward, right, left and backward moves with respect to the last step taken ( $p_{\rightarrow}$ ,  $p_{\downarrow}$ ,  $p_{\uparrow}$  and  $p_{\leftarrow}$ ) and generate a new random walk using this constant transition probabilities, which now do not depend on the concentration field anymore. The MFPT of this effective model can be computed analytically by following the same method as the one introduced in [46] without assuming that the left/right and backward probabilities are equal. The resulting MFPT follows the same trend as the actual

MFPT of the full model but it tends to overestimate the real MFPT, c.f. dotted to solid lines in Fig. 3(a). The difference in the MFPT quantifies the effect of long-term memory for the search efficiency of an auto-chemotactic walker and therefore strongly suggests that long-term memory is beneficial for the single-agent search.

#### IV. THE N-AGENT SEARCH

To quantify the collective search efficiency of  $N$  particles searching for a randomly located target, we compare the mean first-passage (MFPT) of  $N$  interacting searchers  $\bar{T}_N$  to that of  $N$  independent searchers, which only sense their own odor. The MFPT of  $N$  independent searchers can be obtained from the single-searcher simulations. Given  $S_1(t)$ , the survival probability of the target in the single-agent search, the joint survival probability for  $N$  independent processes is given by  $S_N(t) = [S_1(t)]^N$ , leading to a MFPT computed as

$$\bar{T}_N^{\text{ind}} = \int_0^\infty [S_1(t)]^N dt. \quad (9)$$

Note that in case  $S_1(t)$  is a pure exponential decay then  $\bar{T}_N^{\text{ind}} = \bar{T}_1/N$ . We define the ratio  $\bar{T}_N^{\text{ind}}/\bar{T}_N$  as a measure of collective search efficiency.  $\bar{T}_N^{\text{ind}}/\bar{T}_N > 1$  means that collective search is more advantageous than individualistic search and that interaction between agents speeds up the search.

##### A. Many ACPs

In this section we study the collective search efficiency in the ACP model with  $N = 30$  and  $N = 300$  auto-chemotactic particles corresponding to a packing fractions  $\phi \approx 0.01$  and  $\phi \approx 0.1$ , respectively, which is quite dilute such that effects due to the area exclusion are marginal. Because of computational limitations, we mainly focus on  $\phi \approx 0.1$ . Different patterns arise when varying the bare persistence length  $l_p$ , the chemotactic sensitivity  $\beta$  and the parameters of the concentration field ( $D_c$ ,  $k_c$  and  $h_c$ ), see Fig. 4 (a-d) and the corresponding movies in the Supplemental Material [71]. At low  $l_p \approx 0.5$  and not to large dimensionless coupling  $1 \leq \Lambda = \beta h_c a / D_c^2 \leq 10$  particles are homogeneously distributed, see Fig. 4(a). For  $D_c / (v_0 a) \gg 1$  the concentrations profile forms instantly, which in 2d is  $c(r) \propto \exp(-r/\lambda) / \sqrt{r/\lambda}$  for large distances  $r$ , where  $\lambda = \sqrt{D_c / k_c}$ . Consequently, the particles behave as if they would interact via an effective repulsive screened Coulomb potential. With increasing  $\Lambda$  and at similar  $l_p$  small oscillatory bands or exploding clusters appear, see Fig. 4(b). A large-scale pattern emerges at larger  $l_p \approx 5$  and  $10 \leq \Lambda \leq 100$ , where particles move in bands, surfing on a wave of self-generated chemo-repellent spanning the entire length of the box [10], see Fig. 4(c). Small

immobile clusters surrounded by a gas phase of ACP's can be observed at height  $\Lambda > 1000$  and  $l_p > 1$ , see Fig. 4(d). Simple active Brownian particles are slowed down by collisions and small clusters with a lifetime of the order of  $D_\tau^{-1}$  are formed. In ACP, the sensor and source are shifted relative to each other, which leads to an effective alignment by the concentration field of neighboring particles. This stabilizes the small clusters, which usually consist of 3, 4 or 6 particles and form highly symmetrical structures such as triangles or diamonds.

As elaborated above, the MFPT of a single ACP depends essentially on the effective persistence length  $l_p^{\text{eff}}$  and in the following we address the question whether the chemotactic repulsion between the particles change  $l_p^{\text{eff}}$ ? Fig. 5(a) shows  $l_p^{\text{eff}}$  of  $N = 30$  interacting ACP's as a function of  $l_p^{\text{eff}}$  of a single ACP. At small  $\Lambda$  the interactions are unimportant and the points lie on the dashed line, the identity function. With increasing  $\Lambda$ , collisions between particles increase the rotational diffusion and thus reduce the persistence. On the other hand, at large  $\Lambda$ , where immobile clusters form, the persistence is greatly increased due to alignment introduced by neighboring particles. If we plot the MFPT  $\bar{T}_N$  as a function of  $l_p^{\text{eff}}$  for  $N = 30$ , see Fig. 5(b), we observe basically the behavior of a single ACP, but with two main differences. First, the MFPT is much smaller than that of simple active Brownian particles ( $\beta = 0$ ) with the same persistence for a coupling  $\Lambda > 1$ . Second, the search performance decreases significantly for large  $\Lambda > 1000$ , due to trapping of particles into immobile clusters. Bands appear at higher densities since one needs at least  $L/(2a) \approx 50$  particles and will be discussed below.

It is a reasonable assumption that a search process of  $N$  agents is affected by their self-organized spatial arrangement: the more homogeneous the agents are distributed the better the search area can be explored [61]. In order to quantify the homogeneity of the space exploration we use a Voronoi tessellation defining a Voronoi cell for each particle position  $\mathbf{r}_i$ , which contains all points closest to  $\mathbf{r}_i$ . From this we obtain the Voronoi cell's normalized area-distribution function and finally its standard deviation  $\sigma_A^2 = \langle A^2 \rangle - \langle A \rangle^2$  of the normalized cell areas  $A = A/\langle A \rangle$ , where  $\langle A \rangle = L^2/N$  is the mean area. The area-distribution for randomly distributed particles was precisely determined via computer simulation and the estimate of its standard deviation is  $\sigma_A^{\text{ind}} = \sqrt{0.28}$  [72]. We define the measure of the homogeneity of the agent distribution as the ratio  $\sigma_A^{\text{ind}}/\sigma_A$ . For homogeneously distributed particles  $\sigma_A^{\text{ind}}/\sigma_A > 1$  holds and for clustered particles  $\sigma_A^{\text{ind}}/\sigma_A < 1$  [73]. In addition we compute the ratio  $\bar{T}_N^{\text{ind}}/\bar{T}_N$  of the MFPT of  $N$  independent to that of  $N$  interacting searchers. If the collective search efficiency is  $\bar{T}_N^{\text{ind}}/\bar{T}_N > 1$  then collective search is beneficial and the interaction between the agents speeds up search. We combine both quantities, the measure of spatial order  $\sigma_A^{\text{ind}}/\sigma_A$  and the collective search efficiency  $\bar{T}_N^{\text{ind}}/\bar{T}_N$ , together in one diagram for all simulation parameter combinations considered so far, shown in Fig. 6.

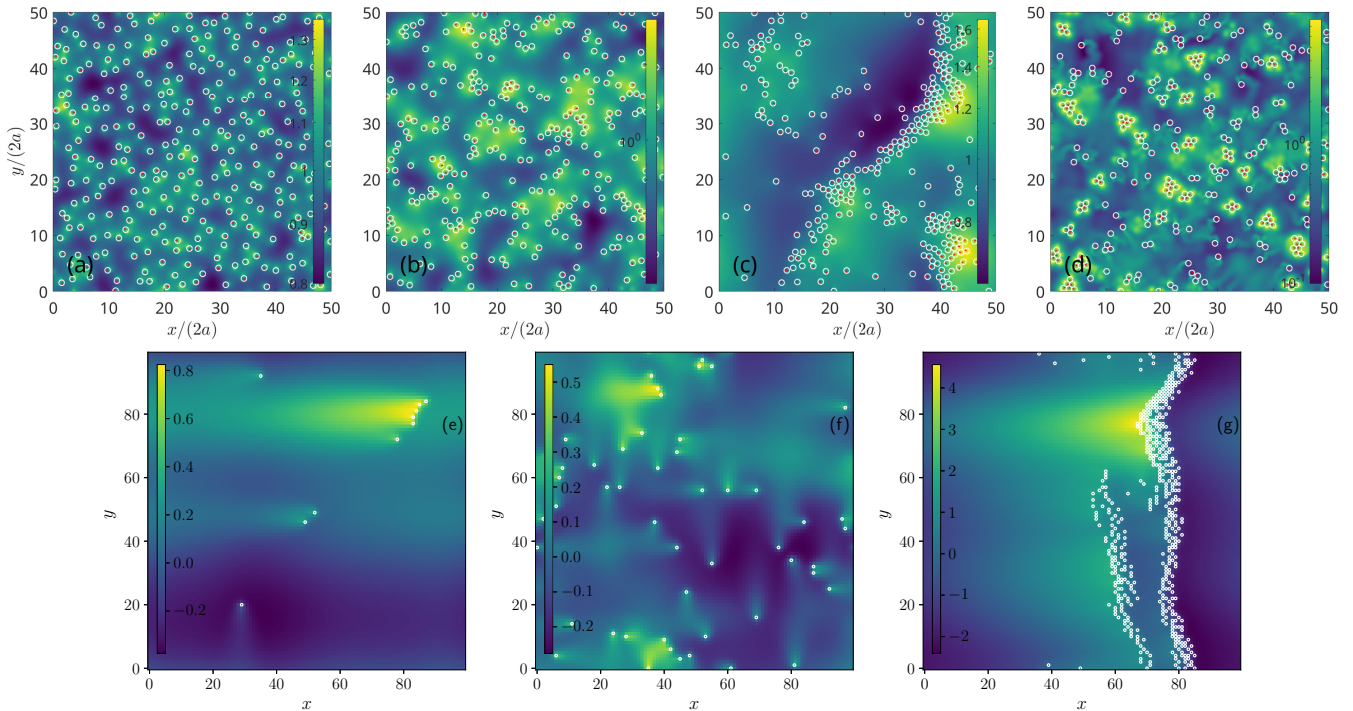


FIG. 4. Simulation snapshots. **Top row:** ACP model with  $N = 300$  autochemotactic particles together with the color-coded concentration field  $\log(c/c_0)$ , where  $c_0 = h_c N / (k_c L^2)$ . The circle indicates the size of the particle and the red arrow its propulsion direction. Lengths are scaled by the radius  $a$  and time by propulsion time  $a/v_0$ . (a) Homogeneously distributed particles ( $l_p, \beta, D_c, k_c, h_c, \Lambda$ ) = **(0.5, 1.25, 10, 0.2, 500, 12.5)**, where  $\Lambda = \beta h_c a / D_c^2$ . (b) Small oscillatory bands **(0.5, 1.25, 2.5, 0.2, 500, 200)**. (c) Travelling bands **(5, 0.125, 2.5, 0.02, 400, 16)**. (d) Immobile clusters **(2.5, 0.25, 0.05, 0.04, 100, 20000)**. **Bottom row:** ACW model for  $D_c = 0.5$ : (e) Flocking phase:  $N = 10$ ,  $\beta = 1000$  - (f) Homogeneous phase:  $N = 50$ ,  $\beta = 100$  - (g) Traveling bands  $N = 500$ ,  $\beta = 1000$ . The background color codes the concentration field while the white circles indicate positions of the walkers. Movies of the simulations are available in the Supplemental Material.

A clear positive correlation between the homogeneity of the spatial particle distribution and the collective search efficiency is observed: the more uniformly the particles are distributed, the higher the search efficiency (i.e. smaller MFPT). The gain in search efficiency due to a homogeneous distribution of the search area among the agents is significant, e.g., it can be up to  $\bar{T}_N \approx 0.4167 \cdot \bar{T}_N^{\text{ind}}$  for  $\phi \approx 0.1$ , see Fig. 6(b). The particles are most homogeneously distributed and hence most effective in search for small  $l_p < 1$  and not too large chemotactic coupling  $\Lambda \approx 10$ . On the other hand, heterogeneously distributed particles forming immobile clusters or traveling bands ( $\sigma_{\mathcal{A}}^{\text{ind}} / \sigma_{\mathcal{A}} < 1$ ) are very ineffective configurations for search, they appear for high persistence  $l_p$  and large coupling strengths  $\Lambda$ .

The gain in search efficiency increases with the density  $\phi$ , c.f. Fig. 6 (a) and (b), which is due to a decreasing mean inter-particle separation and thus a stronger repulsion leading to a more homogeneous particle distribution. Obviously too strong ordering would be disadvantageous, although the search area would be perfectly partitioned among the particles since the particles would tend to localize in the center of their Voronoi-cells, like in

a crystal arrangement, their dynamics would be slowed down and the exploration of the search subarea would be suppressed. In our case, however, none of the uniformly ordered systems showed a dynamical slow-down, neither a subdiffusive region of the mean square displacement nor a decrease in translational diffusion. To maximize the benefit of collective search, it is therefore important that the agents remain in a fluid state, in a delicate balance between partial order and the appropriate level of activity. This is only achieved with low bare persistence  $l_p$  and not too strong coupling to the chemical field.

## B. Many ACWs

Next we examine whether in the ACW model the effective persistence of each searcher is still the essential quantity controlling the search efficiency of a system with  $N$  chemotactically interacting particles, or whether additional collective effects emerge.

*Dilute and homogeneous phases.* At low particle densities, the trend observed for the single-searcher case persists: the MFPT  $\bar{T}_N$  first slowly decreases with

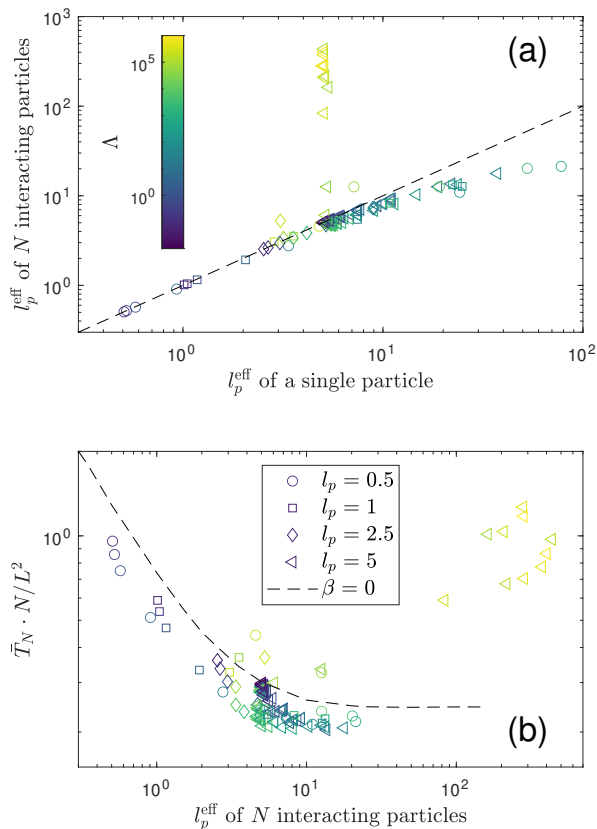


FIG. 5. Many ACPs: (a) Effective persistence length  $l_p^{\text{eff}}$  for the ACP model with  $N = 30$  particles as a function of the effective persistence length  $l_p^{\text{eff}}$  of a single ACP. The dashed line represents  $l_p^{\text{eff}} = l_p$ . The persistence is reduced at intermediate chemotactic coupling strengths  $\Lambda$  due to collisions between particles. At large  $\Lambda$ , immobile clusters form and  $l_p^{\text{eff}}$  is greatly increased. (b) MFPT  $\bar{T}_N$  as a function of  $l_p^{\text{eff}}$  for  $N = 30$  interacting ACPs, scaled with the particle density  $N/L^2$ . The dashed line shows the MFPT of active Brownian particles (ABPs) without coupling to the chemical field ( $\beta = 0$ ). The MFPT of ACPs is smaller than the MFPT of ABPs, except at large  $\Lambda$ , where clustering sets in. Different bare persistence lengths  $l_p$  are indicated by different symbols and the dimensionless chemotactic coupling  $\Lambda = \beta h_c a / D_c^2$  is color-coded.

the chemotactic coupling strength  $\beta$  and then increases abruptly, see Fig 7(a). This suggests that the physical mechanism at play is similar to the one observed for the single-walker search, i.e., the system reaches a state where all walkers move ballistically at large values of  $\beta$ , which leads to a very inefficient search. This phase was documented in Ref. [18], where it is referred to as the *cluster phase* and is basically a flocking phenomenon: particles approaching each other have a high chance of aligning their mutual directions due to the local profile of their combined concentration fields, and then maintaining this common direction thanks to the effective persistence generated by their own field. This leads to the formation of small clusters of particles traveling ballisti-

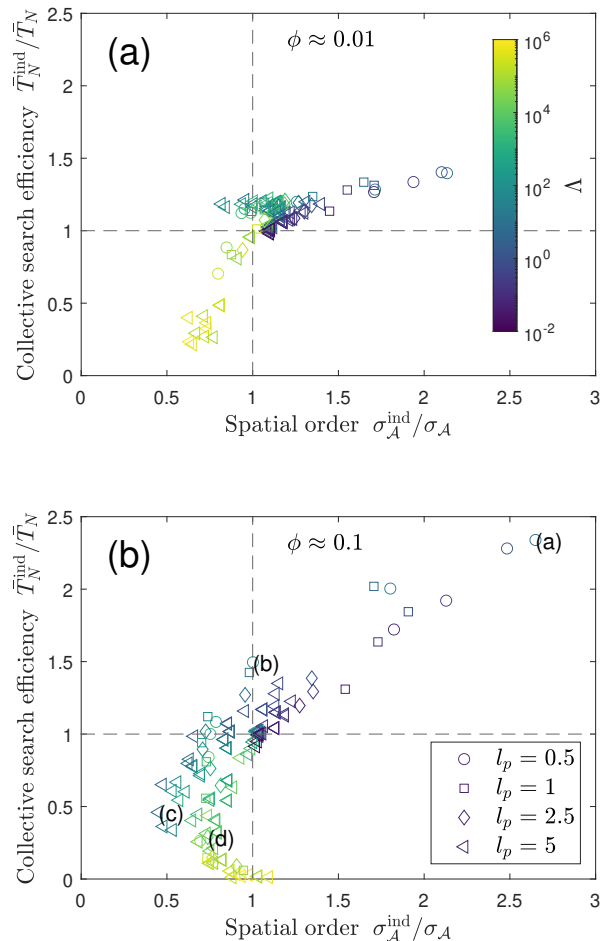


FIG. 6. Many ACPs: Collective search efficiency  $\bar{T}_N^{\text{ind}}/\bar{T}_N$  versus spatial homogeneity  $\sigma_{\mathcal{A}}^{\text{ind}}/\sigma_{\mathcal{A}}$  for two packing fractions (a)  $\phi \approx 0.01$  and (b)  $\phi \approx 0.1$ . Collective search efficiency  $\bar{T}_N^{\text{ind}}/\bar{T}_N$  is defined as the ratio of the mean first passage time of non-interacting  $\bar{T}_N^{\text{ind}}$  to that of interacting particles  $\bar{T}_N$ , i.e., for  $\bar{T}_N^{\text{ind}}/\bar{T}_N > 1$  a collective search is advantageous. Spatial order  $\sigma_{\mathcal{A}}^{\text{ind}}/\sigma_{\mathcal{A}}$  is defined as the ratio of standard deviation of normalized areas  $\mathcal{A} = A/\langle A \rangle$  of non-interacting  $\sigma_{\mathcal{A}}^{\text{ind}}$  (Poisson Voronoi cells) to that of interacting particles  $\sigma_{\mathcal{A}}$ , i.e., for  $\sigma_{\mathcal{A}}^{\text{ind}}/\sigma_{\mathcal{A}} > 1$  the particles are distributed more homogeneous as compared to a spatial Poisson process. Different bare persistence lengths  $l_p$  are indicated by different symbols and the dimensionless chemotactic coupling  $\Lambda = \beta h_c a / D_c^2$  is color-coded. In (b) the letters (a), (b), (c) and (d) correspond to the snapshots in Fig. 4.

cally over large distances, which eventually remain stable once the system has reached a configuration, where they all are far apart from each other, see Fig. 4(e).

At higher densities, the particles constantly collide with each other and do not reach the adsorbing state of the ballistically moving clusters. The system stays in a homogeneous phase, where particles are distributed across space, see Fig. 4(f). As a consequence,  $\bar{T}_N$  does not sharply increase at large values of  $\beta$  but converges to a plateau value for  $\beta \rightarrow \infty$ , which can still be larger than the global minimum reached at a finite value of  $\beta$ ,



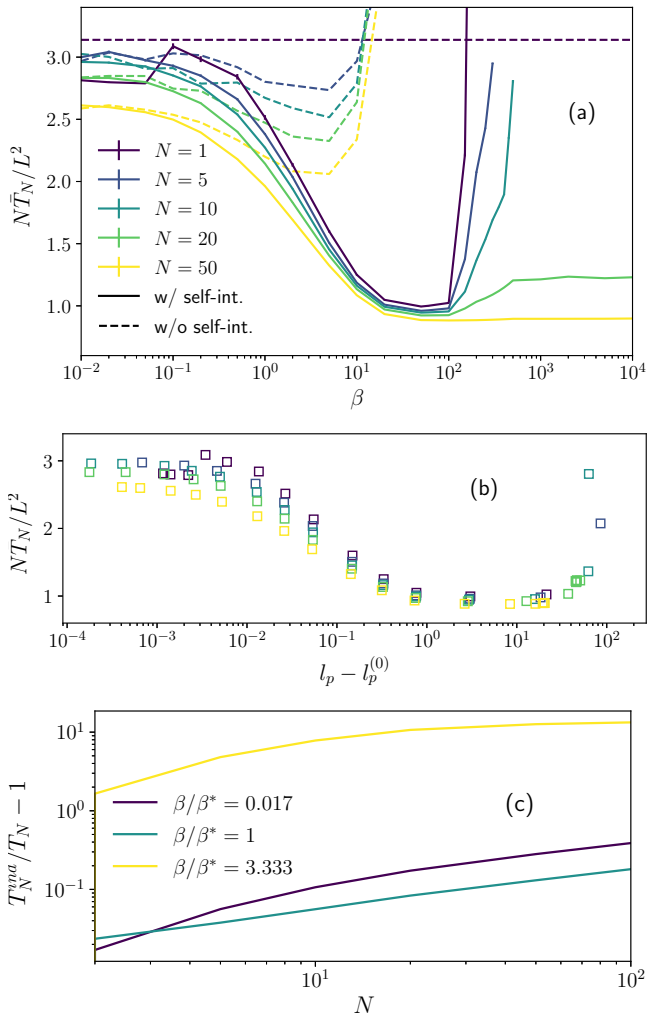


FIG. 7. (a) MFPT  $\bar{T}_N$  of the ACW model for  $D_c = 0.5$  and varying number of walkers  $N$ , both for the original model with self-interaction (solid lines) and for the model where self-interaction is removed, with  $b = 0$  (dashed lines). The value if normalized by  $L^2/N$  for visualization. (b) The same data for  $\bar{T}_N$  in the original model is plotted as a function of the persistence length  $l_p$ , from which the base value  $l_p^{(0)} = 4/3$  is subtracted. (c) Collective search efficiency  $\bar{T}_N^{ind}/\bar{T}_N$  as a function of  $N$  for  $D_c = 0.5$  and various values of  $\beta/\beta^*$ , where  $\beta^*$  is the optimal value of  $\beta$  for the single-agent search.

as shown in Fig 7(a).

Analogous to the single-searcher case one can relate the behavior of the MFPT to the effective persistence length  $l_p$ , as illustrated in Fig. 7(b).  $\bar{T}_N$  evolves again in a non-monotonic way and its minimum is found for a common value  $l_p^*$  regardless of the value of  $N$ , e.g.,  $l_p^* \simeq 10$  for a lattice of size  $L \times L = 100 \times 100$  and  $D_c = 0.5$ . However, it is clear that the persistence length observed for a certain value of  $\beta$  strongly differs for different densities of walkers due to strong interaction effects.

We quantify the influence of interactions using the collective search efficiency  $\bar{T}_N^{ind}/\bar{T}_N$ , which we find to be

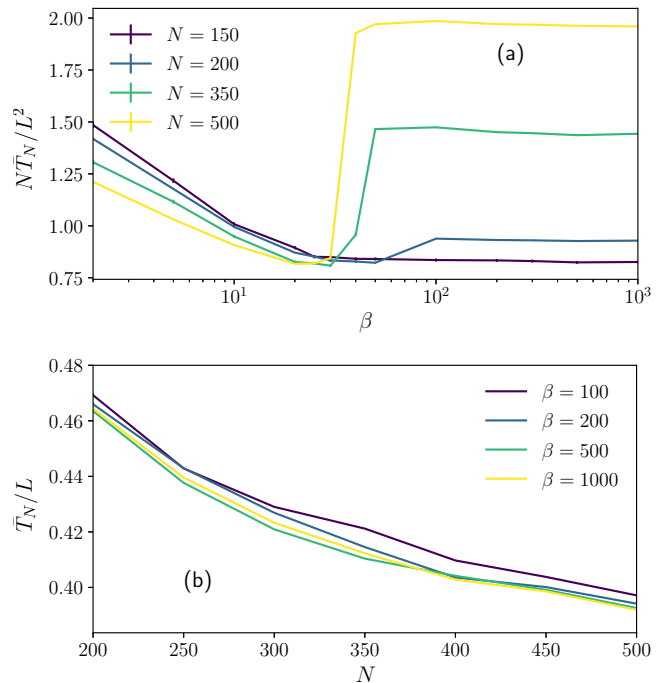


FIG. 8. MFPT  $\bar{T}_N$  of the ACW model for  $D_c = 0.5$  for large number of particles  $N$ . (a)  $\bar{T}_N$  as a function of  $\beta$  for various values of  $N$  (normalized by  $L^2/N$ ). The jump in  $\bar{T}_N$  coincide with the transition from the homogeneous to band phase. (b)  $\bar{T}_N$  as a function of  $\beta$  for various values of  $N$  (normalized by  $L$ ). For a perfect thin band one would expect  $\bar{T}_N = L/2$  independent of  $N$ .

always greater than 1 and to increase with  $N$ , as shown in Fig. 7(c). This indicates that interactions between walkers and their respective fields are beneficial for the search efficiency. Its lowest value is reached when  $\beta = \beta^*$ , i.e. the optimal chemotactic coupling of the single-agent search, indicating that optimal single-agent searches run in parallel is already an overall very efficient strategy. For  $\beta < \beta^*$ , interactions contribute to reducing the search time more, but still by a relatively small amount. Whereas the single-agent search is highly inefficient for  $\beta > \beta^*$ , due to the ballistic motion of the particles, this is no longer the case for the  $N$ -agent process. This results in a very high search efficiency measured by the ratio  $\bar{T}_N^{ind}/\bar{T}_N$  and is a collective effect due to the strong interactions mediated by the chemotactic repulsion.

*Band formation.* At higher densities, the system spontaneously forms macroscopic bands, as reported in Ref. [18]. These bands spread across one axis of the system and travel ballistically in the transverse direction, see Fig. 4(g). There is no limit in the total number of particles they can contain such that one band often contains almost all searchers in the system.

The formation of such structures impacts substantially the mean search time, see Fig. 8(a). While walkers are not well distributed across space, the overall structure traveling at constant speed allows to sweep the system

at once, such that all sites are scanned once the band has traveled across the system. Thus the MFPT is of the order of  $L/2$  and does not vary much with  $N$ , see Fig. 8(b). A more quantitative discussion of the efficiency of searching in a band structure is deferred to section V.

## V. ACW WITHOUT SELF-INTERACTION

So far we have seen that the chemotactic interactions increase the search efficiency of the  $N$ -agent system substantially, but we did not discriminate between the role of the self-interaction and the role of particle-particle interaction. Hence we examine in this section the role of the interaction of the searchers with their own chemotactic field by switching it off. To achieve this one needs to distinguish between the chemotactic field generated by each individual searcher. For simplicity we focus on the ACW model, where the concentration of the chemical produced by searcher  $l$  on site  $j$  is denoted with  $c_j^{(l)}$  and obeys the diffusion equation (7), and the total concentration being  $c_j = \sum_{l=1}^N c_j^{(l)}$ . Switching off the self-interaction means that searcher  $l$  only "sees" the concentration  $c_j - c_j^{(l)}$  replacing  $c_j$  in the exponents of the transition probabilities  $p_{i \rightarrow j}$  in Eq. (6). Since with the self-interaction also the self-induced persistence is switched off we also introduce an additional intrinsic persistence parameter  $b$  and define the probability  $\tilde{p}_{i \rightarrow j}$  for walker  $l$  to jump to a neighboring site  $j$  from a site  $i$  as

$$\tilde{p}_{i \rightarrow j} = \frac{(1 + b_j)e^{-\beta(c_j - c_j^{(l)})}}{\sum_{k \in \mathcal{N}_i} (1 + b_k)e^{-\beta(c_k - c_k^{(l)})}}, \quad (10)$$

where  $b_j = b \geq 0$  if the site  $j$  is the one the walker would reach if he continued in his current direction and  $b_j = 0$  otherwise. Without the interaction with the chemotactic field ( $\beta = 0$ ) the single-walker persistence length is  $l_p = (4 + b)/3$ .

For vanishing intrinsic persistence ( $b = 0$ ) the MFPT is shown in Fig. 7(a) as a function of  $\beta$  for various values of  $N$ . While the case  $N = 1$  leads to a constant value as it simply corresponds to a blind random walk, the behaviour of the curves for  $N > 1$  is significantly different. Starting from the same value as for the case with self-interaction, it then slightly decreases and eventually abruptly increases. This transition occurs at much lower values of  $\beta$  than the transition to the ballistic regime in the original model. This is due to the formation of a frustrated 'crystal-like' state, where each walker is trapped in a cage created by the fields of other walkers. A typical configuration of such state is shown in Fig. 9. In the steady-state, the individual concentration profiles are roughly radially symmetrical and the dynamics of walkers is highly sub-diffusive with even a full dynamical arrest for very large values of  $\beta$ , as can be seen from the behaviour of the mean square displacement in Fig. 10. This results in an extremely large search time  $\bar{T}_N$  for

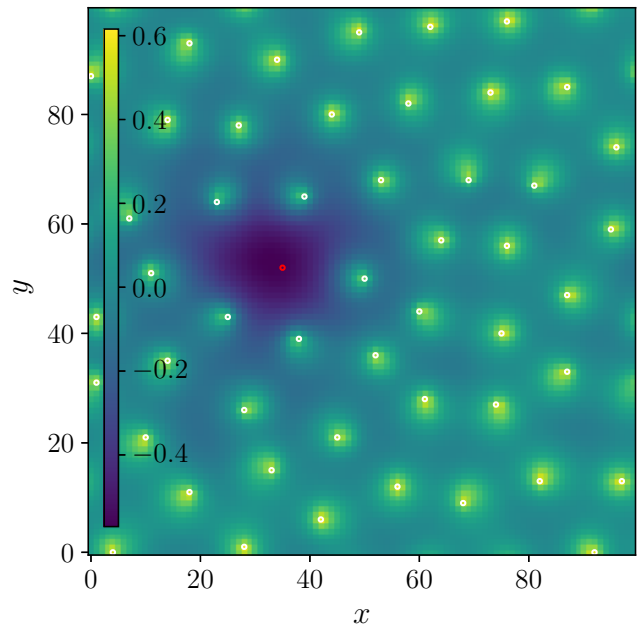


FIG. 9. Simulation snapshot for the ACW model without self-interaction with  $N = 50$ ,  $D_c = 0.5$  and  $\beta = 100$ . The positions of all walkers are indicated with green circles, except for the  $l$ -th walker, represented by a red circle. The background color codes for the concentration field that this specific walker sees, i.e.  $c - c^{(l)}$ . It appears clearly that it is trapped in a cage created by the concentration field of the other walkers. A movie is available in the Supplemental Material.

large values of  $\beta$ , since walkers are essentially immobile and do not scan the domain at all.

An increasing persistence ( $b > 0$ ) allows the walkers to overcome the frustrated state and the system becomes diffusive again (and even super-diffusive at short times), as shown in Fig. 10. Consequently, the MFPT is dramatically influenced by  $b$ . We show in Fig. 11 for  $N = 5$  and  $N = 20$  and various values of  $\beta$  that  $\bar{T}_N$  first strongly decreases with  $b$ , as the system loses its dynamical arrest and becomes more efficient at scanning the domain. Then, for larger values of  $b$ ,  $\bar{T}_N$  increases again as the bias  $b$  is so strong that walkers eventually reach again the ballistic regime and do not feel the effect of the concentration field. There is thus an optimal value of  $b$  that minimizes the MFPT to reach a randomly located target in the biased model without self-interaction.

The value of the MFPT reached at this optimal point can be compared to the value of the MFPT for the same parameter set of the full ACW model with self-interaction, as shown in Fig. 11. At small values of the chemotactic coupling  $\beta$  the ACW model without self-interaction at its optimal bias value performs better than the original model. This is due to the fact that in this region the interaction with the field is rather weak such that making the walkers artificially persistent through an optimal value of  $b$  will make the search more efficient.

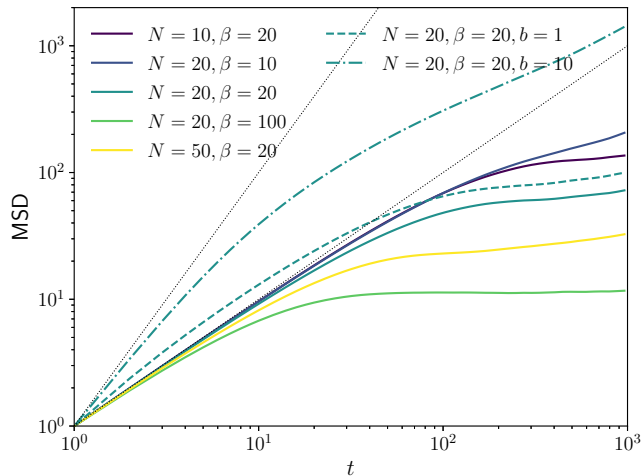


FIG. 10. Mean-square displacement of the ACW lattice model without self-interaction for  $D_c = 0.5$  and various values of  $N$ ,  $\beta$  and the forward bias  $b$  ( $b = 0$  when not indicated). The dotted lines are the functions  $y = t$  and  $y = t^2$ .

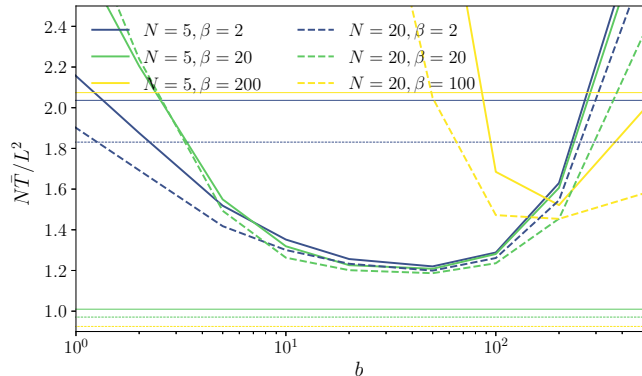


FIG. 11. MFPT of the full ACW model without self-interaction as a function of the persistence parameter  $b$ , for varying searcher number  $N$  and coupling constant  $\beta$ . The corresponding values for the MFPT of the full ACW model are shown for comparison (horizontal lines with same style).

However, in regions where the full ACW model is efficient because of the optimal interaction strength with the field, the ACW model without self-interactions does not outperform the original one. This indicates that the full ACW model, where walkers interact both with their own field but also with the one of other walkers, has intrinsically a superior efficiency for a large range of values of the chemotactic coupling  $\beta$ .

## VI. DISCUSSION

We have revealed a variety of mechanisms rendering non-local, delayed interactions mediated by chemotactic trails beneficial for a collective search, but also scenarios

where the phases emerging from these interactions slow the searchers down.

Most importantly, interactions are beneficial when they allow the searchers to be distributed as uniformly as possible across space, so that each searcher can scan its own sub-area in parallel. This can be achieved by repulsive autochemotaxis, since the repulsive trails the particle left behind, act as an effective repulsive pair potential.

However, being evenly spread across space is not a sufficient condition to be collectively efficient at searching. In fact, searchers also need to be mobile and relatively persistent in order to scan a region of space efficiently. For example, in the frustrated phase in the lattice model without self-interaction, see Fig. 9, the walkers are well distributed across space but almost immobile. Under optimal conditions, assemblies of auto-chemotactic walkers satisfy both conditions: are spontaneously well distributed across space and sufficiently motile to scan space efficiently. This explains why they can be very efficient collective searchers.

For a single ACP reducing the decay rate  $k_c$  of the chemical cue, i.e., making the trails survive longer, improves the search efficiency substantially for large  $\beta$  and small  $D_c$ . However, multiple ACPs in this parameter range mainly form immobile clusters, the worst configuration for effective search, and therefore the positive effect of long-term memory cannot come into play. For a single ACW we showed that long-term memory also significantly reduces the search time by comparing the MFPT of the full model with that of an effective model under the assumption of a short-lived memory. However, in contrast to the ACP, the improvement is present for a much larger range of parameters, even for small  $\beta$  and large  $D_c$ , and long-term memory should thus almost always have a positive effect on collective search.

It should still be noted that both models exhibit the formation of traveling bands, whose search efficiency needs to be addressed in more details, as this strategy is used by humans in some situations such as police search for missing people or rescue of a person buried in an avalanche.

We derive a simple criterion when searching in bands surpass parallel searching of evenly distributed particles: Consider  $N$  searchers with radius  $a$  in a region of size  $L^2$ , which (case A) move homogeneously distributed with an effective diffusion constant  $D_{\text{eff}}$ , or (case B) move in a band spanning the system in a lateral direction (say in  $y$ -direction) with a velocity  $v_0$ . The MFPT in case A can be estimated as

$$\bar{T}_{\text{hom}} = \alpha L^2 / (ND_{\text{eff}}) \quad (11)$$

with some constant  $\alpha$  of order  $\ln L$ . The MFPT of particles moving with velocity  $v_0$  in a band formation (case B) is

$$\bar{T}_{\text{band}} = L / (2v_0). \quad (12)$$

Consequently it is still more efficient to search by uni-

formly distributing agents if

$$\frac{\bar{T}_{hom}}{\bar{T}_{band}} = \frac{2\alpha v_0}{D_{eff}} \cdot \frac{L}{N} < 1, \quad (13)$$

which is fulfilled for a sufficiently large number of diffusive searchers:  $N > L \cdot 2\alpha v_0 / D_{eff}$ . This is plausible since increasing the number  $N$  of searchers in a band simply increases the band thickness such that only the walkers in front of the band are actually scanning new area while the walkers behind only pass over the area that have already been checked.

Several conclusions can be drawn from this estimate. First, at least  $N = L/(2a)$  searchers are needed to form a continuous band (without holes). Even with this minimum number of searchers a diffusive search would still be more efficient than band search if  $4\alpha v_0 a / D_{eff} < 1$ , i.e. for small velocity  $v_0$  or large effective diffusion constant  $D_{eff}$  (as long as the system size  $L$  is fixed since  $\alpha$  grows logarithmically with  $L$ ). Second, for non-interacting ABPs with self-propulsion velocity  $v_0$  and rotational diffusion constant  $D_r$  the effective diffusion constant is  $D_{eff} = v_0^2 / 2D_r$  and the persistent length is  $l_p = v_0 / aD_r$ , such that the criterion for a more efficient diffusive search can be expressed as  $\bar{T}_{hom} / \bar{T}_{band} = 4\alpha L / (l_p a N) < 1$ . As expected  $N$  independent persistent searchers are more efficient than band searchers when their persistent length is sufficiently large (note that this argument only holds as long as  $l_p \ll L$ ). Third, similarly, for the independent persistent random walkers (i.e the autochemotactic searcher with  $\beta = 0$ ) the persistence length is  $p_{\rightarrow} / (1 - p_{\rightarrow})$ , where  $p_{\rightarrow}$  is the persistence probability, i.e. the probability to move in the same direction as in the last step, and the effective diffusion constant  $D_{eff} = \gamma l_p^2$  with some prefactor  $\gamma$ . Again the criterion for a more efficient diffusive search can be expressed as  $\bar{T}_{hom} / \bar{T}_{band} = 2\alpha L / (\gamma l_p N) < 1$  (where we set the lattice constant  $a = 1$ ). Fourth, most relevant for our results on the MFPT of the collective  $N$ -particle search is that once the chemotactically interacting searchers form bands, these bands are substantially broader than minimally needed ( $N \gg L/(2a)$ ). As our estimate (13) predicts, the MFPT then becomes much larger than the MFPT for particles being homogeneously distributed over the search area. Thus, the criterion (13) explains the sharp increase of MFPT at the transition from the homogeneous to band phase, which gets stronger with increasing  $N$ , see Fig. 8(a).

## VII. CONCLUSION

Our work shows that chemotactic interactions among motile agents allow collective search strategies of superior efficiency due to mainly three reasons: First, the traces left by particles along their trajectory act as an effective memory, preventing agents from visiting the same location twice within a short period of time. Second, the

self-interaction of the agents with their own chemotactic field leads to an effective persistence length of the trajectories that can be beneficial for the search. Third, the chemotactic interaction of agents with the trails of other searchers leads to more homogeneous spatial distribution of the searchers and thus to a more efficient space exploration in the search for the randomly located target. Moreover, we found that the spontaneous formation of ballistically moving bands, although commonly applied in search-and-rescue operations, is mostly not beneficial for the search process due to the large number of agents necessary to sustain the band pattern induced by chemotactic interactions.

Our study is the first to comprehensively explore the impact of complex interactions on collective search strategies on the micro-scale for which reason a plethora of variations and extensions remain unexplored and deserve further investigation.

So far, we have looked at particles that secrete repulsive chemical signals, but there is also evidence that some cells can create gradients themselves by degrading an attractant in their environment, thus acting as sinks rather than sources [5, 6]. These situations are not dual to each other because the concentration of an attractant cannot become negative, for which reason new collective effects might emerge.

Moreover, beyond chemotaxis, which is a directed response to chemical gradients, many microorganisms exhibit chemokinesis, which is an undirected response to changes in chemical concentration. This behavior involves altering speed or reorientation frequency based on the locally sensed concentration of chemicals. For example, the bacteria *Myxococcus xanthus*, which is well-known for its predatory behavior on other microorganisms, exhibits in addition to auto-chemotaxis also auto-chemokinesis [74]. However, the impact of auto-chemokinesis on collective search remains unexplored.

With regards to applications to foraging organisms one should also think about more complex chemical clues, containing more information, like a time-stamp or directional information, or influencing also searcher speed or persistence.

In conclusion this work combines two major research areas: active matter with its recent exploration of chemotactic active colloids or droplets, migrating cells, and living organisms; and stochastic processes and search strategies with its recent focus on non-Markovian search processes. Hence our study of collective search strategies of large groups of interacting agents might not only be relevant for chemotactic active matter but also for a wide range of fields like ethology [75], information engineering [76], robotics [77], and social engineering [78].

## VIII. ACKNOWLEDGMENTS

We acknowledge financial support by the DFG via the Collaborative Research Center SFB 1027.

- [1] D. Helbing, A. Dussutour, V. Fourcassié and J.-L. Deneubourg. Optimal traffic organization in ants under crowded conditions. *Nature*, 428:70–73, 2004.
- [2] Erika Donà, Joseph D. Barry, Guillaume Valentin, Charlotte Quirin, Anton Khmelinskii, Andreas Kunze, Sevi Durdu, Lionel R. Newton, Ana Fernandez-Minan, Wolfgang Huber, Michael Knop, and Darren Gilmour. Directional tissue migration through a self-generated chemokine gradient. *Nature*, 503(7475):285–289, 2013.
- [3] Bruna A. David and Paul Kubers. Exploring the complex role of chemokines and chemoattractants in vivo on leukocyte dynamics. *Immunological Reviews*, 289(1):9–30, 2019.
- [4] Carolyn E Adler, Richard D Fetter, and Cornelia I Bargmann. Unc-6/netrin induces neuronal asymmetry and defines the site of axon formation. *Nature Neuroscience*, 9(4):511–518, 2006.
- [5] Luke Tweedy, David A. Knecht, Gillian M. Mackay, and Robert H. Insall. Self-generated chemoattractant gradients: Attractant depletion extends the range and robustness of chemotaxis. *PLOS Biology*, 14:1–22, 03 2016.
- [6] Luke Tweedy, Peter A. Thomson, Peggy I. Paschke, Kirsty Martin, Laura M. Machesky, Michele Zagnoni, and Robert H. Insall. Seeing around corners: Cells solve mazes and respond at a distance using attractant breakdown. *Science*, 369(6507):eaay9792, 2020.
- [7] Joseph d’Alessandro, Alex Barbier-Chebbah, Victor Cellerin, Olivier Benichou, RenéMarc Mège, Raphaël Voituriez, and Benoît Ladoux. Cell migration guided by long-lived spatial memory. *Nature Communications*, 12(1):4118, 2021.
- [8] Babak Vajdi Hokmabadi, Jaime Agudo-Canalejo, Suropriya Sahab, Ramin Golestanian, and Corinna C. Maass. Chemotactic self-caging in active emulsions. *Proc. Nat. Acad. Sci. USA*, 119:e2122269119, 2022.
- [9] Bokusui Nakayama, Hikaru Nagase, Hiromori Takahashi, and Toshiharu Saiki. Tunable pheromone interactions among microswimmers. *Proc. Nat. Acad. Sci. USA*, 120:e2213713120, 2023.
- [10] Benno Liebchen, Davide Marenduzzo, and Michael E. Cates. Phoretic interactions generically induce dynamic clusters and wave patterns in active colloids. *Phys. Rev. Lett.*, 118:268001, 2017.
- [11] Benno Liebchen and Hartmut Löwen. Synthetic chemotaxis and collective behavior in active matter. *Accounts of Chemical Research*, 51(12):2982–2990, 2018.
- [12] Jens Grauer, Hartmut Löwen, Avraham Be’er, and Benno Liebchen. Swarm hunting and cluster ejections in chemically communicating active mixtures. *Scientific Reports*, 10(1):5594, 2020.
- [13] W Till Kranz and Ramin Golestanian. Trail-mediated self-interaction. *The Journal of Chemical Physics*, 150(21), 2019.
- [14] Babak Vajdi Hokmabad, Jaime Agudo-Canalejo, Suropriya Saha, Ramin Golestanian, and Corinna C Maass. Chemotactic self-caging in active emulsions. *Proceedings of the National Academy of Sciences*, 119(24):e2122269119, 2022.
- [15] Zahra Mokhtari, Robert IA Patterson, and Felix Höfling. Spontaneous trail formation in populations of auto-chemotactic walkers. *New Journal of Physics*, 24(1):013012, 2022.
- [16] A Barbier-Chebbah, O Bénichou, and R Voituriez. Self-interacting random walks: Aging, exploration, and first-passage times. *Physical Review X*, 12(1):011052, 2022.
- [17] Eduardo Moreno, Robert Großmann, Carsten Beta, and Sergio Alonso. From single to collective motion of social amoebae: a computational study of interacting cells. *Frontiers in Physics*, 9:750187, 2022.
- [18] Hugues Meyer and Heiko Rieger. Alignment interaction and band formation in assemblies of autochemorepulsive walkers. *Phys. Rev. E*, 108:034604, Sep 2023.
- [19] A. V. Ivlev, J. Bartnick, M. Heinen, C.-R. Du, V. Nosenko, and H. Löwen. Statistical mechanics where newton’s third law is broken. *Phys. Rev. X*, 5:011035, 2015.
- [20] Zhihong Youa, Aparna Baskaranb, and M. Cristina Marchetti. Nonreciprocity as a generic route to traveling states. *Proc. Nat. Soc. USA*, 117:19767–19772, 2020.
- [21] Ramin Golestanian Suropriya Saha, Jaime Agudo-Canalejo. Scalar active mixtures: The nonreciprocal cahn-hilliard model. *Phys. Rev. X*, 10:041009, 2020.
- [22] Michel Fruchart, Ryo Hanai, Peter B Littlewood, and Vincenzo Vitelli. Non-reciprocal phase transitions. *Nature*, 592(7854):363–369, 2021.
- [23] Jyoti Prasad Banerjee, Rituparno Mandal, Deb Sankar Banerjee, Shashi Thutupalli, and Madan Rao. Unjamming and emergent nonreciprocity in active ploughing through a compressible viscoelastic fluid. *Nature Communications*, 13:4533, 2022.
- [24] Leanid Laganenka, Remy Colin, and Victor Sourjik. Chemotaxis towards autoinducer 2 mediates autoaggregation in escherichia coli. *Nature Communications*, 7(1):12984, 2016.
- [25] Elva J. H. Robinson, Duncan E. Jackson, Mike Holcombe, and Francis L. W. Ratnieks. ‘no entry’ signal in ant foraging. *Nature*, 438(7067):442–442, 2005.
- [26] Timothy H Chung, Geoffrey A Hollinger, and Volkan Isler. Search and pursuit-evasion in mobile robotics: A survey. *Autonomous robots*, 31:299–316, 2011.
- [27] N. G. van Kampen. *Stochastic Processes in Physics and Chemistry*. North-Holland, Amsterdam, 1992.
- [28] S. Redner. *A Guide to First-Passage Processes*. Cambridge University Press, Cambridge, 2001.
- [29] Paul C. Bressloff. *Stochastic Processes in Cell Biology*. Springer, Heidelberg, 1992.
- [30] M.V. Smoluchowski. Versuch einer mathematischen theorie der koagulationskinetik kolloider lösungen. *Z. Phys. Chem.*, 92:129–168, 1917.
- [31] F.C. Collins and G.E. Kimball. Diffusion-controlled reaction rates. *Colloid Sci.*, 4:425–439, 1949.
- [32] S.A. Rice. *Diffusion-Limited Reactions*. Elsevier, Amsterdam, 1985.
- [33] P. H. von Hippel O. G. Berg, R. B. Winter. Diffusion-driven mechanisms of protein translocation on nucleic acids. 1. models and theory. *Biochemistry*, 20:6929–6948, 1981.
- [34] Jason Gorman and Eric C Greene. Visualizing one-dimensional diffusion of proteins along dna. *Nature structural & molecular biology*, 15(8):768–774, 2008.
- [35] H. C. Berg. *E. Coli in motion*. Springer, Heidelberg, 2005.

- [36] Matthew F Krummel, Frederic Bartumeus, and Audrey Gérard. T cell migration, search strategies and mechanisms. *Nature Reviews Immunology*, 16(3):193–201, 2016.
- [37] MP Hassell and TRE Southwood. Foraging strategies of insects. *Annual review of ecology and systematics*, 9(1):75–98, 1978.
- [38] James FA Traniello. Foraging strategies of ants. *Annual review of entomology*, 34(1):191–210, 1989.
- [39] Andrew M Edwards, Richard A Phillips, Nicholas W Watkins, Mervyn P Freeman, Eugene J Murphy, Vsevolod Afanasyev, Sergey V Buldyrev, Marcos GE da Luz, Ernesto P Raposo, H Eugene Stanley, et al. Revisiting lévy flight search patterns of wandering albatrosses, bumblebees and deer. *Nature*, 449(7165):1044–1048, 2007.
- [40] Thomas T Hills, Christopher Kalff, and Jan M Wiener. Adaptive lévy processes and area-restricted search in human foraging. *PLoS One*, 8(4):e60488, 2013.
- [41] Madhubhashi Senanayake, Ilankaikone Senthoran, Jan Carlo Barca, Hoam Chung, Joarder Kamruzzaman, and Manzur Murshed. Search and tracking algorithms for swarms of robots: A survey. *Robotics and Autonomous Systems*, 75:422–434, 2016.
- [42] Daniel S Drew. Multi-agent systems for search and rescue applications. *Current Robotics Reports*, 2:189–200, 2021.
- [43] Hugues Meyer and Heiko Rieger. Should you hire new searchers? optimal number of agents in a collective search, and when to launch them. *arXiv preprint arXiv:2401.05851*, 2024.
- [44] Michael A Lomholt, Koren Tal, Ralf Metzler, and Klafter Joseph. Lévy strategies in intermittent search processes are advantageous. *Proceedings of the National Academy of Sciences*, 105(32):11055–11059, 2008.
- [45] Olivier Bénichou, Claude Loverdo, Michel Moreau, and Raphael Voituriez. Intermittent search strategies. *Reviews of Modern Physics*, 83(1):81, 2011.
- [46] Vincent Tejedor, Raphael Voituriez, and Olivier Bénichou. Optimizing persistent random searches. *Physical review letters*, 108(8):088103, 2012.
- [47] Hugues Meyer and Heiko Rieger. Optimal non-markovian search strategies with n-step memory. *Physical Review Letters*, 127(7):070601, 2021.
- [48] Anton Klimek and Roland R Netz. Optimal non-markovian composite search algorithms for spatially correlated targets. *Europhysics Letters*, 139(3):32003, 2022.
- [49] Lukasz Kusmierz, Satya N Majumdar, Sanjib Sabhapanidit, and Grégory Schehr. First order transition for the optimal search time of lévy flights with resetting. *Physical review letters*, 113(22):220602, 2014.
- [50] A Chechkin and IM3845437 Sokolov. Random search with resetting: a unified renewal approach. *Physical review letters*, 121(5):050601, 2018.
- [51] Paul C Bressloff. Search processes with stochastic resetting and multiple targets. *Physical Review E*, 102(2):022115, 2020.
- [52] Aleksander Stanislavsky and Aleksander Weron. Optimal non-gaussian search with stochastic resetting. *Physical Review E*, 104(1):014125, 2021.
- [53] Ofir Tal-Friedman, Arnab Pal, Amandeep Sekhon, Shlomi Reuveni, and Yael Roichman. Experimental realization of diffusion with stochastic resetting. *The journal of physical chemistry letters*, 11(17):7350–7355, 2020.
- [54] Amy Altshuler, Ofek Lauber Bonomo, Nicole Goro-hovsky, Shany Marchini, Eran Rosen, Ofir Tal-Friedman, Shlomi Reuveni, and Yael Roichman. Environmental memory facilitates search with home returns. *arXiv preprint arXiv:2306.12126*, 2023.
- [55] S. Redner and P. L. Krapivsky. Capture of the lamb: Diffusing predators seeking a diffusing prey. *American Journal of Physics*, 67:1277–1283, 1999.
- [56] P. L. Krapivsky G. Oshanin, O. Vasilyev and J. Klafter. Survival of an evasive prey. *Proc. Nat. Acad. Soc. USA*, 106:13696, 2009.
- [57] Carlos Mejía-Monasterio, Gleb Oshanin, and Grégory Schehr. First passages for a search by a swarm of independent random searchers. *Journal of Statistical Mechanics: Theory and Experiment*, 2011(06):P06022, 2011.
- [58] A. Nandi Nayak and D. Das. Capture of a diffusive prey by multiple predators in confined space. *Phys. Rev. E*, 102:062109, 2020.
- [59] G. Oshanin D. S. Grebenkov, R. Metzler. From single-particle stochastic kinetics to macroscopic reaction rates: fastest first-passage time of n random walkers. *New J. Phys.*, 22:103004, 2020.
- [60] D. S. Grebenkov. Depletion of resources by a population of diffusing species. *Phys. Rev. E*, 105:54402, 2022.
- [61] Noriyuki P. Tani, Alan Blatt, David A. Quint, and Ajay Gopinathan. Optimal cooperative searching using purely repulsive interactions. *Journal of Theoretical Biology*, 361:159–164, 2014.
- [62] Sunghan Ro, Juyeon Yi, and Yong Woon Kim. Target searches of interacting brownian particles in dilute systems. *Phys. Rev. E*, 107:064143, Jun 2023.
- [63] Ricardo Martínez-García, Justin M Calabrese, Thomas Mueller, Kirk A Olson, and Cristóbal López. Optimizing the search for resources by sharing information: Mongolian gazelles as a case study. *Physical Review Letters*, 110(24):248106, 2013.
- [64] Pawel Romanczuk, Markus Bär, Werner Ebeling, Benjamin Lindner, and Lutz Schimansky-Geier. Active brownian particles: From individual to collective stochastic dynamics. *The European Physical Journal Special Topics*, 202:1–162, 2012.
- [65] M. R. Shaebani, A. Wysocki, R. G. Winkler, G. Gompfer, and H. Rieger. Computational models for active matter. *Nat. Rev. Phys.*, 2:181, 2020.
- [66] Holger Stark Johannes Taktikos, Vasily Zaburdaev. Collective dynamics of model microorganisms with chemotactic signaling. *Phys Rev E*, 85:051901, 2012.
- [67] Daniel J Amit, Giorgio Parisi, and Luca Peliti. Asymptotic behavior of the “true” self-avoiding walk. *Physical Review B*, 27(3):1635, 1983.
- [68] Johannes Taktikos, Vasily Zaburdaev, and Holger Stark. Modeling a self-propelled autochemotactic walker. *Phys. Rev. E*, 84:041924, Oct 2011.
- [69] Katherine Daftari and Katherine A. Newhall. Self-avoidant memory effects on enhanced diffusion in a stochastic model of environmentally responsive swimming droplets. *Phys. Rev. E*, 105:024609, Feb 2022.
- [70] W.H. Press. *Numerical Recipes 3rd Edition: The Art of Scientific Computing*. Numerical Recipes: The Art of Scientific Computing. Cambridge University Press, 2007.
- [71] See Supplemental Material at [URL will be inserted by publisher] for Videos S1–S6 of the numerical simulations corresponding to the snapshots in Fig. 4 and Fig. 9.
- [72] Járjai-Szabó Ferenc and Zoltán Néda. On the size distribution of poisson voronoi cells. *Physica A: Statistical Mechanics and its Applications*, 385(2):518–526, 2007.

- [73] R. Monchaux, M. Bourgoïn, and A. Cartellier. Preferential concentration of heavy particles: A Voronoï analysis. *Physics of Fluids*, 22(10):103304, 10 2010.
- [74] David R Zusman, Ansley E Scott, Zhaomin Yang, and John R Kirby. Chemosensory pathways, motility and development in *myxococcus xanthus*. *Nature Reviews Microbiology*, 5(11):862–872, 2007.
- [75] M. Beekman, D. J. T. Sumpter, and F. L. W. Ratnieks. Phase transition between disordered and ordered foraging in pharaoh’s ants. *Proc. Natl. Acad. Sci. U. S. A.*, 98:9703–9706, 2001.
- [76] M. Dorigo, V. Maniezzo, and A. Coloni. Ant system: Optimization by a colony of cooperating agents. *IEEE Trans. Syst. Man, Cybern. Part B Cybern.*, 26:29–41, 1996.
- [77] M. J. B. Krieger, J. B. Billeter, and L. Keller. Ant-like task allocation and recruitment in cooperative robots. *Nature*, 406:992–995, 2000.
- [78] J. Li and B. Wei. Urban-rural bus path planning based on ant colony optimization algorithm. *Int. Arch. Photogramm. Remote Sens. Spat. Inf. Sci. - ISPRS Arch.*, 42:451–456, 2020.